Energy Engineering

Tech Science Press

DOI: 10.32604/ee.2024.055535

ARTICLE

Maximum Power Point Tracking Based on Improved Kepler Optimization Algorithm and Optimized Perturb & Observe under Partial Shading Conditions

Zhaoqiang Wang[1] **and Fuyin Ni**[2,*]

[1]School of Electrical and Information Engineering, Jiangsu University of Technology, Changzhou, 213001, China

[2]Jiangsu Key Laboratory of Power Transmission & Distribution Equipment Technology, Jiangsu University of Technology, Changzhou, 213001, China

[*]Corresponding Author: Fuyin Ni. Email: dxnfy@jstu.edu.cn

Received: 30 June 2024 Accepted: 02 August 2024 Published: 22 November 2024

ABSTRACT

Under the partial shading conditions (PSC) of Photovoltaic (PV) modules in a PV hybrid system, the power output curve exhibits multiple peaks. This often causes traditional maximum power point tracking (MPPT) methods to fall into local optima and fail to find the global optimum. To address this issue, a composite MPPT algorithm is proposed. It combines the improved kepler optimization algorithm (IKOA) with the optimized variable-step perturb and observe (OIP&O). The update probabilities, planetary velocity and position step coefficients of IKOA are nonlinearly and adaptively optimized. This adaptation meets the varying needs of the initial and later stages of the iterative process and accelerates convergence. During stochastic exploration, the refined position update formulas enhance diversity and global search capability. The improvements in the algorithm reduces the likelihood of falling into local optima. In the later stages, the OIP&O algorithm decreases oscillation and increases accuracy. compared with cuckoo search (CS) and gray wolf optimization (GWO), simulation tests of the PV hybrid inverter demonstrate that the proposed IKOA-OIP&O algorithm achieves faster convergence and greater stability under static, local and dynamic shading conditions. These results can confirm the feasibility and effectiveness of the proposed PV MPPT algorithm for PV hybrid systems.

KEYWORDS

PV hybrid inverter; kepler optimization algorithm; maximum power point tracking; perturb and observe

Nomenclature

$I = I_{pv}$	PV system output current (A)
$V = V_{pv}$	PV system output current (V)
P_{pvout}	PV system output power (W)
X (g)	IKOA planets or solar positions
V (g)	IKOA planetary velocity
F_g (g)	IKOA planets and sun gravity

1 Introduction

With advancements in technology, the efficiency and reliability of photovoltaic (PV) inverters have markedly improved [1]. Features such as maximum power point tracking (MPPT) [2] and remote monitoring have significantly enhanced the widespread adoption of PV power systems. However, traditional PV inverters are limited to converting DC power from solar energy to AC power and cannot store excess energy, which leads to unstable power supply during low-light conditions [3].

With the development of energy storage technology [4] and the reduction of battery costs, energy storage and bi-directional charging and discharging functions [5] can be integrated in PV inverters. In the article, these devices are referred to as PV hybrid inverters. PV hybrid inverters overcome the limitations of traditional PV inverters [6] by storing surplus power for later use, thereby improving system stability, reliability and overall energy efficiency. PV hybrid inverters offer consistent power supply and enhance grid quality, which support the expansion of renewable energy and the development of smart grids [7]. However, the issue of power output variability due to PV panel shading remains a challenge, which impacts the efficiency and performance of PV hybrid inverters [8].

Changes in ambient temperature and light can easily affect PV cell power output. Partial shading conditions (PSC) [9], which are caused by tree shading, cloud shading and ash accumulation [10], make light distribution uneven [11]. MPPT technology aims to keep the PV array operating at the maximum power point (MPP), adapting to changes in temperature and light intensity to quickly find the optimal point. MPPT technology greatly reduces power loss. Traditional methods like the constant voltage method, short-circuit current method, perturbation observation method [12] and conductance increment method [13] work well under consistent light conditions, but struggle with local shading, leading to local optima due to multiple peaks in the output curve [9,14].

To address this, intelligent algorithms such as the particle swarm algorithm (PSO) [14], grey wolf optimization (GWO) algorithm [15], horse herd optimization algorithm (HOA) [16], cuckoo search (CS) algorithm [10], flower pollination algorithm [17] and kepler optimization algorithm (KOA) [18] have been proposed. Literature [14] proposed that a dual optimization particle swarm algorithm optimizes the voltage interval for the MPP and enhances convergence with optimized coefficients and a search degree factor. Literature [15] proposed that an improved gray wolf optimization algorithm with variable-step perturbation observation improves search efficiency and global randomness to avoid local optima. Literature [16] proposed that the horse herd optimization algorithm achieves fast convergence with minimal computation. Literature [10] proposed an adaptive differential evolution of the improved cuckoo search algorithm combined with the conductance incremental method balances search efficiency and randomness. Literature [18] proposed that the KOA uses planetary motion principles for position and velocity updates. These approaches optimize local shading problems, but still struggle to balance output stability with speed and accuracy under various environmental conditions.

This paper proposes a composite algorithm that combined the improved kepler optimization algorithm (IKOA) and the optimized variable-step perturbation observation method (OIP&O). IKOA is used for global optimization in early iterations, adjusting switching probabilities and orbital motion step coefficients adaptively. Early iterations use a smaller switching probability and a larger step coefficient to promote global search, while later iterations use a larger switching probability and a smaller step coefficient to enhance accuracy and convergence speed. The velocity and position update formulas are optimized to increase diversity and improve the ability to escape local optima, which enhance global search randomness. In later stages, the algorithm switches to OIP&O for local optimization, which reduces output oscillation and improves stability and accuracy. Simulation and

experimental results confirm the correctness and effectiveness of this PV MPPT algorithm for the PV hybrid inverter.

This paper is structured as follows, Section 2 describes the PV hybrid inverter system modeling and presents its main combinatorial elements to introduce the PV array that is the object of study. Section 3 describes the basics of PV modeling and analyzes the effect of PSC on the power output of the PV array. The IKOA-OIP&O algorithm and the corresponding MPPT process are presented in Section 4. Experimental results by the proposed algorithm and comparison between different algorithms are given in Section 5. The paper is summarized in Section 6.

2 PV Hybrid Inverter System Design

PV hybrid inverter is a smart energy solution that utilizes solar power to generate electricity and realizes power storage and power supply management [19], through bi-directional inverter and energy storage system, as shown in Fig. 1. PV hybrid inverter mainly consists of PV battery system, energy storage battery system, bi-directional inverter and so on.

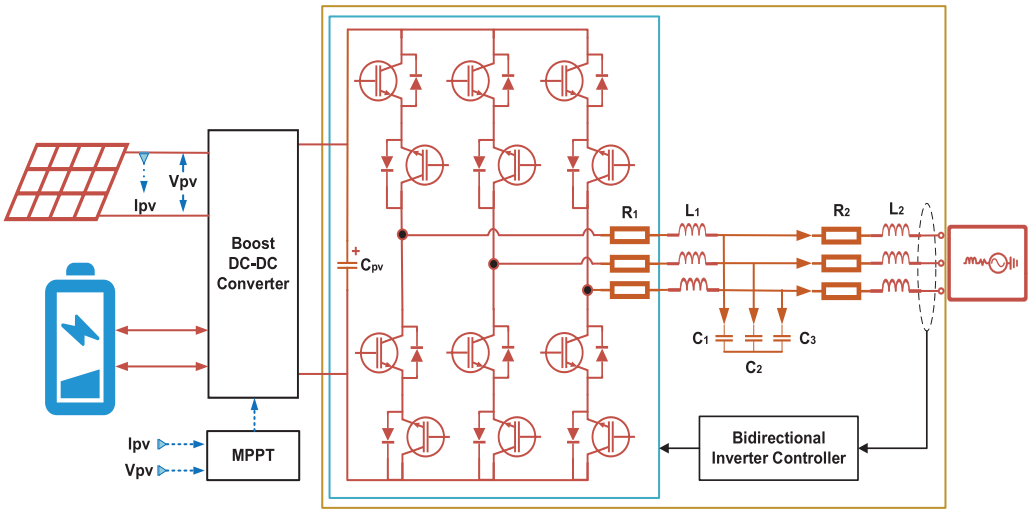

Figure 1: PV hybrid inverter system

The PV cell system in a PV hybrid inverter is a technological device that converts solar energy into electrical energy and consists mainly of PV panels, boosting circuits and a MPPT controller [11]. It converts solar energy directly into usable DC energy through the PV effect, which is then passed through an inverter for domestic and commercial use [5,6]. PV cell systems can reduce carbon emissions, realize sustainable use of energy, and bring economic benefits through reduced electricity bills and revenue from electricity sales, providing users with a stable and reliable power supply [1,20].

The storage battery system in a PV hybrid inverter is a device for storing and managing the electrical energy generated by PV panels [7]. It includes a battery module, a battery management system (BMS) and bi-directional charging and discharging circuits [5]. Its main function is to store excess electrical energy during the day for use at night or on cloudy days to ensure the continuity and stability of power supply. The system effectively improves the overall efficiency of the PV hybrid inverter, reduces dependence on the grid, optimizes energy utilization and provides a backup power function, thus enhancing the reliability and economy of the energy system.

The bi-directional inverter circuit in a PV hybrid inverter is a power electronic device capable of realizing bi-directional conversion between DC and AC power [7]. It includes a bidirectional DC/AC converter [21], an inverter module and a control system [22]. As the demand for energy storage and management continues to rise, bidirectional converters are poised to become a critical technology for optimizing electrical energy utilization and enhancing system flexibility and efficiency [23]. These converters not only facilitate efficient bidirectional conversion of PV power but also provide precise control between energy storage and release, addressing power demand fluctuations and improving system reliability [7].

3 PV Component Models

PV panels, which are crucial components of PV hybrid inverters, have primarily been categorized into single-sided and bifacial panels [20] to improve PV conversion efficiency [24]. Bifacial panels can simultaneously receive light from both the front and back sides, resulting in higher current and power output under identical illumination conditions compared to single-sided panels [25]. However, the output characteristic curves (I-V and P-V curves) of both types are very similar in shape, with the curves of bifacial panels being steeper and more efficient. Due to this similarity, it is feasible to approximate the output curves of bifacial panel arrays under shading conditions using those of single-sided panel arrays. Therefore, the focus of this study will primarily be on single-sided PV panels. PV panels have P-U and I-U output curves that are greatly affected by light intensity and operating ambient temperature. the equivalent model of PV cells is shown in Fig. 2.

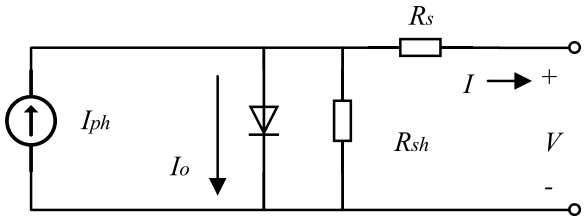

Figure 2: Equivalent model diagram of PV modules

The expression for the output current is shown below [20]:

$$I = I_{ph} - I_d \left\{ \exp\left[\frac{q\,(V + IR_s)}{AkT_{pv}} \right] - 1 \right\} - \frac{V + IR}{R_{sh}} \tag{1}$$

where I_{ph} for the photogenerated current; I for the PV module output current; V for the PV module output voltage I_d for the diode reverse saturation current; R_s and R_{sh} for the equivalent series resistance and the equivalent parallel resistance; k for Boltzmann's constant, the value of which is usually 1.38 $\times$ 10^{23} J/K; q for the electronic charge constant, the value of which is usually 1.6 $\times$ 10^{19} C; A for the ideal factor of the PN junction, and T_{pv} for the absolute temperature.

$$I_{ph} = \left[I_{sc} + K_i \left(T_{pv} - T_r \right) \right] \frac{S}{S_r} \tag{2}$$

where I_{sc} for the short-circuit current in the standard operating environment; K_i for the short-circuit current temperature coefficient; T_r for the standard operating temperature (25°C); S_r for the standard

light intensity (1000 W/m^2); S is the work of light intensity (W/m^2). Saturation current expression:

$$I_d = I_{do}\left\{\exp\left[\frac{q\,(V+IR_s)}{AKT}\right]-1\right\} \tag{3}$$

where I_{do} is the saturation current at standard conditions.

The PV array is made of N_s individual cells connected in series with the following output current equation:

$$I = I_{ph} - I_d\left[\exp\left(\frac{q\,(V+IR_s)}{N_sAkT}\right)-1\right] - \frac{V+N_sIR_s}{N_sR_{sh}} \tag{4}$$

In the simulation to build a PV cell model, set up five PV panels connected in parallel as a group, a total of five groups connected in series in turn, components arranged PV arrays, and change the lighting conditions, the temperature is constant 25°C. The key parameters of a single PV cell (TSM-200DA01.08) as shown in Table 1.

Table 1: Key parameters of PV cells

Parameter name	Parameter value
Open-circuit voltage U_{oc}/V	46.2
MPP voltage U_{mp}/V	38.2
Short-circuit current I_{sc}/A	5.62
MPP current I_{mp}/A	5.26
U_{oc} temperature coefficient /(%/°C)	−0.35
I_{sc} temperature coefficient /(%/°C)	0.05

PV systems are usually operated in natural environments, so the power output is generally nonlinear. When the illumination is uneven due to natural factors, especially the PV cells are greatly affected by temperature and illumination in the environment, the P-U output curve will show a phenomenon of multiple peaks. If the peaks do not differ much, it will increase the probability of falling into the local optimum solution and also trigger the hot spot effect. In order to avoid the hot spot effect, a bypass diode is usually connected in parallel next to the PV array, and the presence of the bypass diode will also make the P-V output characteristics of the PV array characterized by multiple peaks.

4 Implementation of IKOA-OIP&O Based Multi-Peak MPPT Algorithm

4.1 Improved Kepler Optimization Algorithm

Inspired by Kepler's laws of planetary motion, the KOA is a novel meta-heuristic optimization algorithm [18]. KOA simulates the interaction between the sun and the planets, provides an intuitive optimization method using the natural laws of celestial motion. It has good global search capability for the PV maximum power tracking problem in PV hybrid inverters, and avoids the probability of falling into a local optimum through the introduction of stochastic perturbations that can be mentioned [26,27].

However, the traditional KOA is computationally large due to the complexity of simulating planetary motions, leading to slow convergence, as well as the complex optimization problem, although

random perturbations are introduced, it is still easy to fall into the local optimal solution, which is difficult to jump out of [27]. At the same time, in order to target the specific scenario of the PV maximal power tracking, it is necessary to modify and adjust the parameters of the KOA algorithm (e.g., the number of planets, the initial speed, the strength of the perturbations, etc.).

In order to effectively balance the relationship between the search accuracy and convergence speed of the KOA algorithm, the convergence speed and stability of the algorithm are improved while maintaining the global search capability of the algorithm. The IKOA algorithm is described below:

4.1.1 IKOA Parameter Initialization Settings

As shown in Fig. 3, the IKOA algorithm has to initialize the positions of the individual planets in the search space, i.e., the target duty cycle, whose position equations are shown in Eq. (5):

$$X_i = X_{i,lb} + r_0 \times \left(X_{i,ub} - X_{i,lb}\right) \tag{5}$$

where $X_{i,ub}$ and $X_{i,lb}$ are the upper and lower bounds of the search space, respectively; r_0 are random numbers between 0 and 1. It is also necessary to initialize other parameters, such as the orbital parameters e and the orbital period T, which need to be initialized before the optimization starts. The orbital eccentricity and orbital period initialization equations are shown below [18]:

$$e_i = r_1 \tag{6}$$

$$T_i = |r_n| \tag{7}$$

where r_1 is a random number from 0 to 1; r_n is a random number based on a normal distribution.

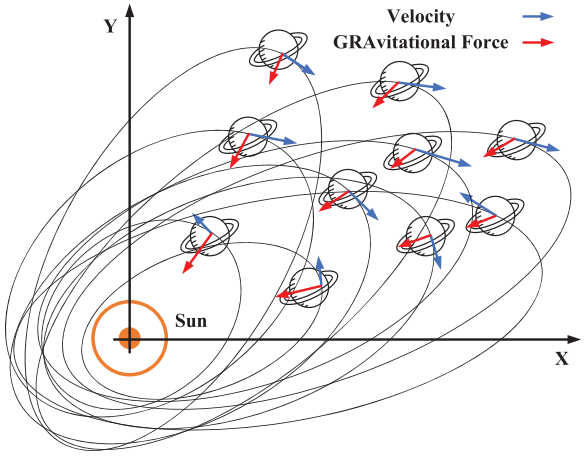

Figure 3: Schematic diagram of the position of the planets in relation to the sun

4.1.2 Calculation of IKOA Gravitational Force

The gravitational force F_g of the planet relative to the Sun is calculated, as follows [18]:

$$F_{g,1}(t) = e_i \times \mu(t) \times \frac{\overline{M}_s \times \overline{m}_i}{\overline{R}_i^2 + \varepsilon} + r_2 \tag{8}$$

where $\mu(t)$ is a function of exponentially decreasing with time, used to control the search precision, defined as shown in Eq. (15); $\overline{M}_s$ and $\overline{m}_i$ denote the normalized values of the masses M_s and of m_i the sun X_s and planets X_i, respectively, calculated according to Eqs. (11) and (12); r_2 denoted by a random number between 0 and 1; $\overline{R}_i$ denoted by the Euclidean distance of the sun X_s and the planets X_i; R_i denoted by the Euclidean normalized distance; ε denoted by a small value to avoid being divided by zero is a small value to avoid division by zero; The Euclidean distance between the Sun and the planets and the related parameters can be calculated from Eqs. (9) to (14) as follows [18]:

$$R_i(t) = \|X_S(t) - X_i(t)\| = \sqrt{\left(X_S(t) - X_i(t)\right)^2} \tag{9}$$

$$\overline{R}_i = \frac{R_i(t) - \min\left(R(t)\right)}{\max\left(R(t)\right) - \min\left(R(t)\right)} \tag{10}$$

$$M_S = r_3 \frac{fit_S(t) - worst(t)}{\sum_{k=1}^{N}\left(fit(t) - worst(t)\right)} \tag{11}$$

$$m_i = \frac{fit_i(t) - worst(t)}{\sum_{k=1}^{N}\left(fit_k(t) - worst(t)\right)} \tag{12}$$

$$\mu(t) = \mu_0 \times \exp\left(-\gamma \frac{t}{T_{\max}}\right) \tag{13}$$

where r_3 is a random number in the range of 0∼1; M_S denoted as the quality of the sun X_s; m_i denoted as the quality of the planet X_i; γ is a fixed value; μ_0 is an initial value; t and $T_{\max}$ denotes the current iteration number and the maximum iteration number, respectively; $fit(t)$ and $worst(t)$ are calculated as shown below [18]:

$$fit_S(t) = best(t) = \max_{k\in[1,\ 2,\cdots,N]}\left(fit_k(t)\right) \tag{14}$$

$$worst(t) = \min_{k\in[1,\ 2,\cdots,N]}\left(fit_k(t)\right) \tag{15}$$

4.1.3 Calculation of Planetary Orbital Velocities in IKOA

The planetary velocity is calculated by the distance from the sun, and the planetary velocity increases as the planet gets closer to the sun and decreases as it gets farther away from the sun. In the traditional KOA, the planetary velocity update step parameter is a fixed value of 1 or −1. The step size of planetary velocity update is too large, which leads to the results of skipping the optimal solution, slower convergence, oscillations or discretization, and lower accuracy. In order to ensure that the algorithm has a sufficient search range and at the same time ensure a fine search near the optimal solution, the planetary velocity update step size is improved by nonlinearly incrementing in the range of 0∼1. In turn, according to the Vis-viva equation [18], the velocity of the planet relative to the Sun, modified based on the MPPT, is shown in Eqs. (16) to (27) [18]:

$$V_i(t) = \begin{cases} l \times (2 \times r_5 \times X_i - X_b) + \ddot{l} \times (X_a - X_b) + \\ (1 - R_{i-norm}(t)) \times \alpha_t \times U_1 \times \vec{r}_6 \times \left(X_{i,\ ub} - X_{i,\ lb}\right), & R_{i-norm}(t) \le 0.5 \\ r_5 \times L \times (X_a - X_i) + \\ (1 - R_{i-norm}(t)) \times \alpha_t \times U_2 \times \vec{r}_6 \times \left(r_4 \times X_{i,\ ub} - X_{i,\ lb}\right), & R_{i-norm}(t) > 0.5 \end{cases} \tag{16}$$

$$l = U \times M \times L \tag{17}$$

$$L = \left[\mu\left(t\right) \times \left(M_s + m_i\right)\left(\frac{2}{R_i\left(t\right) + \varepsilon} - \frac{1}{a_i\left(t\right) + \varepsilon}\right)\right]^{\frac{1}{2}} \tag{18}$$

$$M = \left(r_4 \times \left(1 - r_5\right) + r_5\right) \tag{19}$$

$$U = \begin{cases} 0 & r_6 \le r_7 \\ 1 & r_6 > r_7 \end{cases} \tag{20}$$

$$\ddot{l} = \left(1 - U\right) \times M \times L \tag{21}$$

$$U_1 = \begin{cases} 0 & r_6 \le r_5 \\ 1 & r_6 > r_5 \end{cases} \tag{22}$$

$$U_2 = \begin{cases} 0 & r_4 \le r_5 \\ 1 & r_4 > r_5 \end{cases} \tag{23}$$

where $V_i\left(t\right)$ indicates the current planetary velocity; r_4, r_5, r_6 and r_7 are random numbers in the range 0 to 1; X_a and X_b are two random solutions in the current solution; $a_i\left(t\right)$ is the half-length axis of the elliptical orbit of the *ith* celestial planets, which can be calculated by Eq. (24); α_t is the planetary velocity update step, which can be calculated by Eq. (25); $R_{i-norm}\left(t\right)$ denotes the normalization of the Euclidean distance between a celestial body X_s and X_i, which can be calculated by Eq. (26).

$$a_i\left(t\right) = r_4 \times \left[T_i^2 \times \frac{\mu\left(t\right) \times \left(M_s + m_i\right)}{4\pi^2}\right] \tag{24}$$

$$\alpha_t = R_{i-norm} \times \alpha_{\max} \times \left(\frac{\alpha_{\min}}{\alpha_{\max}}\right)^{\frac{t}{T_{\max}}} \tag{25}$$

where $\alpha_{\max}$ and $\alpha_{\min}$ are the upper and lower step values, respectively.

$$R_{i-norm}\left(t\right) = \frac{R_i\left(t\right) - \min\left(R\left(t\right)\right)}{\max\left(R\left(t\right)\right) - \min\left(R\left(t\right)\right)} \tag{26}$$

The purpose of Eq. (26) is to calculate the percentage of steps in which each object undergoes a change; if $R_{i-norm}\left(t\right) \le 0.5$, then the celestial planet is close to the sun and will increase its speed to prevent drifting towards the sun due to the sun's immense gravitational pull. Otherwise, the celestial planet will slow down.

4.1.4 Escape from IKOA Local Optimization

The improved adaptive perturbation switching probability facilitates the optimal solution to jump out of the local optimum at a later stage of the algorithm. In the traditional KOA, the normalized Euclidean distance between a celestial body and the condition for judgment is fixed, typically 0.5, so that the probability of updating the planetary velocity is the same throughout the iteration period.

Therefore, this paper proposes an adaptive probability P_{r-norm}. In the early stage of the algorithm operation, in order to improve the global search ability and increase the search range, a larger value P_{r-norm} is needed; in the late stage of the algorithm operation, in order to improve the search accuracy and accelerate the convergence speed, a smaller value P_{r-norm} is needed. The proposed formula for adaptive is:

$$P_{r-norm} = 0.7 - 0.4\,(T_{\max} - t)\,/\,T_{\max} \tag{27}$$

where t is the number of iterations at the current moment; $T_{\max}$ is the maximum number of iterations.

4.1.5 Update of Planetary Positions in IKOA

Escaping the local optimum, as shown in Fig. 4, by simulating the gravitational pull of the Sun on the planet, the local optimum region is broken through by periodically switching the search direction to provide the planet with a better chance to explore the whole space. The exploration operation is simulated in IKOA when the planets are farther away from the sun, while the mining operation is realized when the planets are closer to the sun. The positions are updated as shown below [18]:

$$X_i\,(t+1) = X_i\,(t) + P_{r-norm} \times V_i\,(t) + \left(F_{g,\,i}\,(t) + |r_8|\right) \times U \times (X_s\,(t) - X_i\,(t)) \tag{28}$$

where r_8 is a random number from 0 to 1.

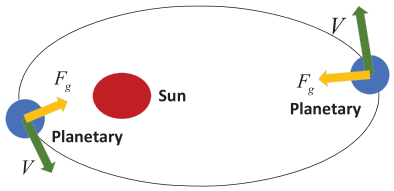

Figure 4: Exploration and exploration of planets in search space

The positions of the celestial planets are updated to simulate the natural change in the distance between the sun and the planets over time. As the planets get closer to the sun, the mining operator is activated to increase the rate of convergence, while when the sun is farther away, The exploration operator is activated to minimize falling into a local optimum, as shown below [18]:

$$X_i\,(t+1) = X_i\,(t) \times U_1 + (1 - U_1) \times \left(\frac{X_i\,(t) + X_S + X_a\,(t)}{3.0} + h \times \left(\frac{X_i\,(t) + X_S + X_a\,(t)}{3.0} - X_b\,(t)\right)\right) \tag{29}$$

where h is the adaptive factor for the distance between the Sun and the current planet at the control moment t, as shown in the following equation [18]:

$$h = \frac{1}{e^{\eta r_9}} \tag{30}$$

where r_9 is the randomized number of the normal distribution, η is a linear decreasing factor from 1 to -2, as shown in the following equation [18]:

$$\eta = (a_2 - 1) \times r_{10} + 1 \tag{31}$$

where r_{10} is a random number from 0 to 1, a_2 is the control parameter, as shown in the following equation:

$$a_2 = -1 - 1 \times \left(\frac{t\%_0 \dfrac{T_{\max}}{\overline{T}}}{\dfrac{T_{\max}}{\overline{T}}} \right) \tag{32}$$

where $\overline{T}$ is the number of cycles control parameter.

When the number of iterations of the above IKOA algorithm reaches a set value and the tracking is near the current MPP, in order to further improve the accuracy of the algorithm in tracking the maximum power, an optimized variable-step perturbation algorithm is used to perform a small-scale local search to find the global MPP.

4.2 Optimized Variable-Step Perturbation Observation Method Algorithm Implementation

The P&O perturbation observation method is one of the commonly used MPPT methods, which has the characteristics of easy implementation and simplicity, and can help the optimization algorithm's further search for the optimal point. However, the traditional P&O perturbation method, its step size is usually a constant fixed value. If the step size is set too small, it will reduce the search speed and lead to a long convergence time; when the step size is set too large, it will lead to large fluctuations at the MPP, which reduces the accuracy of the search. Therefore, in this paper, an OIP&O is used to improve the perturbation step size by sampling the PV system, which is comparing and calculating the output power and output voltage before and after the perturbation and their change rates to optimize the step size, and the perturbation process is shown in the following equation:

$$\begin{cases} P_{pv,\ out} = U_{pv} \times I_{pv} \\ \Delta P_{pv,\ out} = P_{pv,\ out}(i) - P_{pv,\ out}(i-1) \\ \Delta U_{pv}(i) = U_{pv}(i) - U_{pv}(i-1) \\ \Delta D(k) = \left| \Delta P_{pv,\ out}(i) / \Delta U_{pv}(i) \right| \times \Delta D \end{cases} \tag{33}$$

where U_{pv} and I_{pv} are the output voltage and current of the PV system; $P_{pv,\ out}(i)$ and $P_{pv,\ out}(i-1)$ are the power values before and after the *ith* perturbation, separately; $\Delta P_{pv,\ out}$ is the power increment before and after the perturbation. $\Delta U_{pv}(i)$ is the value of the output voltage change caused by the duty cycle change from time $k-1$ to time k; $\Delta D(k)$ is the value of the duty cycle change step at time k; ΔD is the value of the fixed duty cycle change, which is a fixed value. If $\Delta P_{pv,\ out}$ is positive after perturbation, the next perturbation will be made in the same direction; if $\Delta P_{pv,\ out}$ is negative after perturbation, the next perturbation will be made in the opposite direction.

The OIP&O initially approaches the MPP faster by a larger amount of perturbation. After successfully tracking near the MPP, the reduction of power variation and voltage variation causes the perturbation amount to be reduced accordingly, thus improving the tracking accuracy.

4.3 Algorithm Restart Condition

For the MPPT control strategy algorithm, it is necessary to ensure that the whole system works at the MPP in real time, but the sudden change of the external environment often affects the output power of the system, in order to avoid the loss of power to ensure the stable operation of the system, the restart of the algorithm is also very important. This paper adopts the absolute magnitude of the fluctuation of the output power of the PV array and the ratio of the maximum output power.

Under the working conditions as the restart conditions, that is, to meet Eq. (34) when the algorithm restarts [28].

$$\frac{\left|P_{real}-P_{mppt}\right|}{P_{mppt}}>\lambda \tag{34}$$

where P_{real} is the real-time output power of the PV panel; P_{mppt} is the maximum output power searched by the algorithm under the current working condition; λ is the occupancy factor, $\lambda = 0.04$.

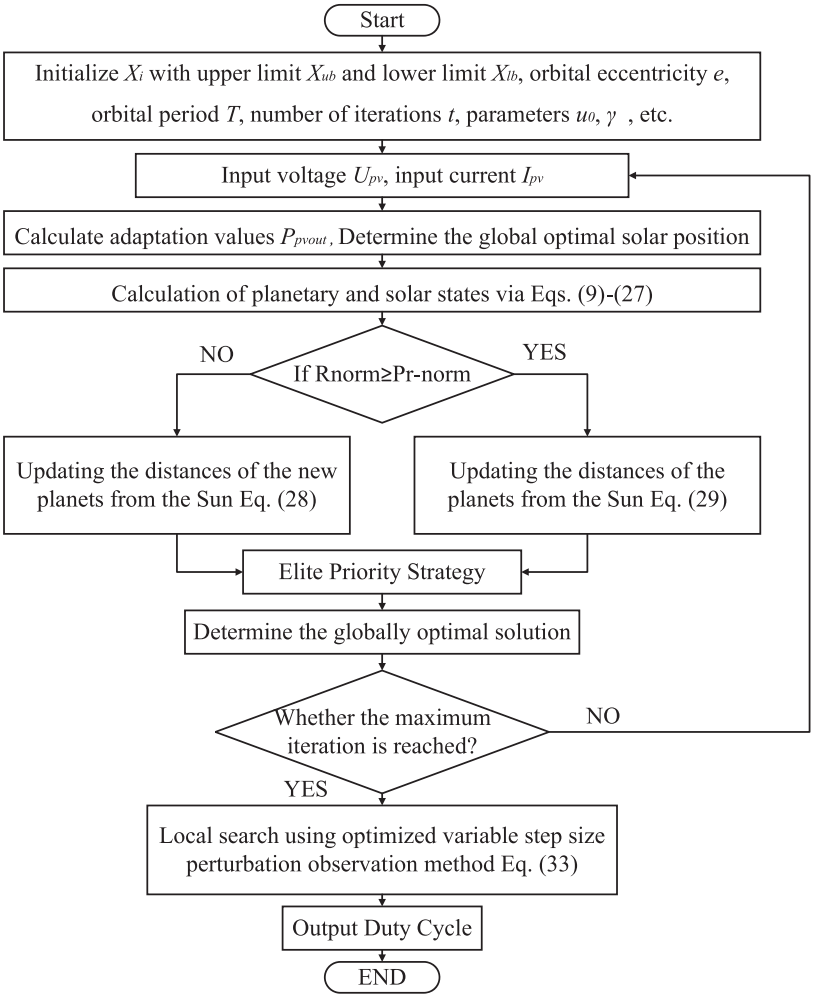

Figure 5: Flowchart of IKOA-OIP&O algorithm

In summary, as shown in the algorithm flowchart in Fig. 5 below. In the early stage of this paper, the IKOA algorithm is used as a means of global search, and the initial planetary population position, spatial upper bound, spatial lower bound, orbital parameters and orbital period are generated, according to the improved Kepler algorithm. The search and exploration of the solution space are carried out to determine the value of the maximum PV power and the corresponding duty cycle, through the optimal strategy. Subsequently, an OIP&O is adopted to locally search the current optimal duty cycle, in order to improve the search accuracy of the PV MPP. Then the algorithm restart setting is carried out. The planet position represents the duty cycle of the Boost circuit, which realizes the

maximum power tracking control and eliminates the traditional PI control loop, simplifying the design and operation of the controller.

5 Algorithm Simulation Results and Simulation

In order to verify the effectiveness and performance of the present proposed improved Keplerian algorithm, simulations are carried out in Simulink. The PV array consists of 5 × 5 module blocks with individual module parameters $P_{\max} = 200.932$ W, $V_{oc} = 46.2$ V, $I_{sc} = 5.62$ A, $V_m = 38.2$ V, $I_m = 5.26$ A. The Boost converter parameters are PV side boost capacitance $C_{pv} = 1000$ uF, Load-side capacitance $C = 200$ uF, $L = 10$ mH. The key parameters of the IKOA-OIP&O algorithm are shown in Table 2:

Table 2: IKOA-OIP&O algorithm main parameters

	Statuses	Value		Statuses	Value
1	Duty cycle	100.0	6	γ	15
2	Duty cycle	10.0	7	$\overline{T}$	3
3	μ_0	0.1	8	$T_{\max}$	10
4	$X_{i,\ ub}$	0.90	9	C_{pv}	1000 uF
5	$X_{i,\ lb}$	0.10	10	L	10 mH

In order to specifically analyze the multi-peak output characteristics of PV arrays under localized PSC, the localized shading conditions are simulated by giving four groups of PV cells set with different light intensities, respectively. In order to highlight the impact of localized shading on PV arrays, the environmental parameters are set as shown in Table 3, with the STC as the unshaded state, the set light intensity of 1000 constant and the temperature of 25°C.

The P-U and I-U characteristic curves of the PV array under four working conditions are shown in Fig. 6. As can be seen from Fig. 6, under working condition I (uniform illumination), the P-U characteristic curve of the PV array has only one peak point, and the traditional MPPT algorithm can effectively track to the MPP. However, under working condition PSC1, PSC2 and PSC3, due to changes in the external environment (light intensity, temperature, etc.), the P-U characteristic curve of the PV array is a nonlinear curve with multiple peak points, but there is one and only one global MPP. Therefore, in order to ensure that the PV array can always work at the MPP under complex operating conditions, the study of PV multi-peak MPPT is of great significance.

Table 3: Environmental parameter settings

Statuses	PV1	PV2	PV3	PV4	PV5
STC	1000	1000	1000	1000	1000
PSC1	1000	800	600	400	200
PSC2	900	700	500	300	100
PSC3	1000	800	500	700	1000

The simulation environment is selected to be at 25°C, and a total of four states are simulated, so that the PV arrays are simulated under the two conditions of standard working condition (STC) and

switching to working condition PSC1 (uniform illumination and localized shade), and the mutation of working condition PSC1 to working condition PSC2, and then to working condition PSC3 (dynamic shading), and the simulation experiments are conducted to compare the same conditions of CS, GWO-P&O, KOA-P&O, and IKOA-OIP&O algorithms under the same conditions, and analyze the convergence speed and tracking accuracy of the algorithms.

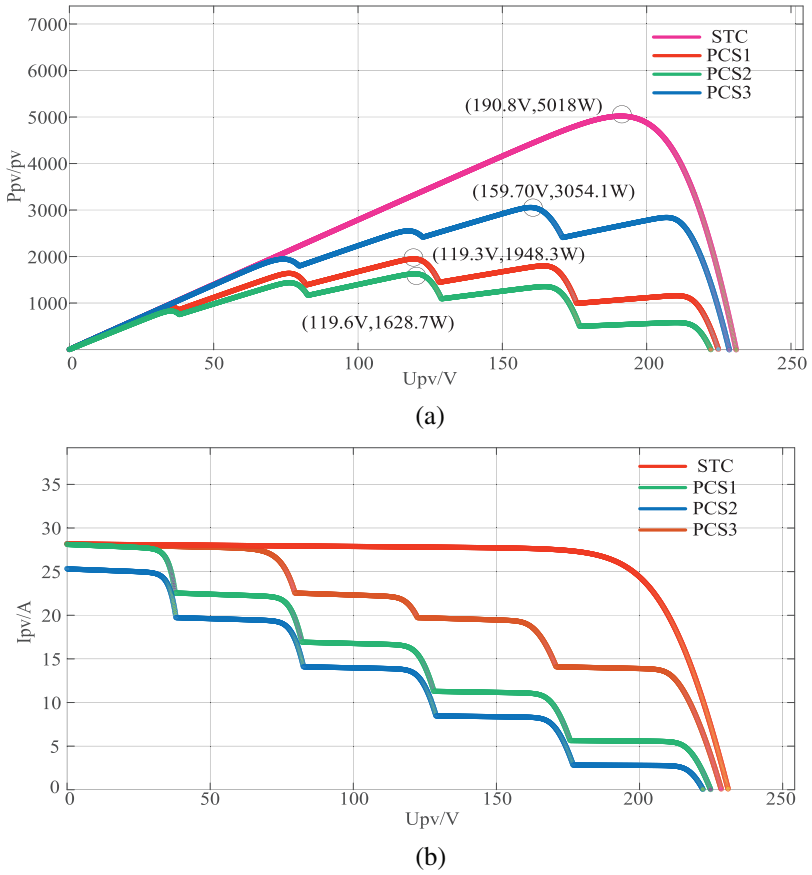

Figure 6: Characteristic curve of PV array output power under different working conditions. (a) U-I characteristic curves for four operating conditions. (b) P-U characteristic curves for four operating conditions

This study evaluates a proposed MPPT algorithm in comparison with three existing methods designed for PV panel output characteristics: CS algorithm, Grey Wolf Optimization-Perturb and Observe (GWO-P&O), and kepler optimization algorithm-perturb and observe (KOA-P&O). The CS algorithm, known for its simplicity and reliability, may exhibit slower dynamic response and instability under varying PV conditions. This comparison assesses the advancements achieved over these traditional methods.

The GWO-P&O and KOA-P&O algorithms, representing recent advancements in optimization, aim to enhance MPPT efficiency and accuracy for PV panels. Despite their improvements, these methods may face higher computational complexity and adaptability challenges. By contrasting the proposed algorithm with these advanced methods, strengths in dynamic response, tracking accuracy,

and computational efficiency are highlighted, demonstrating its practical value and potential for further research and application in optimizing PV panel performance.

5.1 Uniform Light and Partial Shade

When the PV array is working in uniform illumination (STC), the PV power output curve has only one peak. At this time, the maximum power of the system is 5018 W. The IKOA-OIP&O algorithm is simulated and output, and the three algorithms of CS, GWO-P&O, and KOA-P&O are compared, and the simulation time reaches 1 s when switching to the PSC1 condition, as shown in Fig. 7, the PV power output presents multiple peaks, and when the peaks do not have much difference, it will appear to fall into the local optimal The maximum power of the system is 1948.3 W. The simulation results of the four algorithms are shown in Fig. 6, and the simulation results of STC and PSC1 are shown in Table 4 and Fig. 8.

Table 4: Simulation results of the algorithm under uniform light and local shade conditions

State mode	Algorithm	Maximum power/W	Tracking power/W	Tracking rate/%	Tracking time/s
STC	CS	5018	4996.1	99.56	0.62
	GWO-P&O	5018	4996.6	99.57	0.42
	KOA-P&O	5018	4996.7	99.57	0.92
	IKOA-OIP&O	5018	4996.9	99.57	0.39
PSC1	CS	1948.3	1934.9	99.31	0.12
	GWO-P&O	1948.3	1935.9	99.36	0.66
	KOA-P&O	1948.3	1790.1	91.88	0.48
	IKOA-OIP&O	1948.3	1936.1	99.37	0.38

From Figs. 7, 8 and Table 4, it can be seen that: in the initial STC for maximum power tracking, CS system finds the optimal value around 0.62, and the optimal value is around 4996.1 W; GWO-P&O finds the optimal value (around 4996.6 W) around 0.42 s; KOA-P&O system finds the optimal value (around 4996 W) in approximately 0.6 s. the system based on IKOA-OIP&O finds the optimal value around 0.39 s, and the optimal value is around 4996.9 W. It can be seen that IKOA-OIP&O algorithm is better than the other three algorithms in terms of optimization speed and accuracy.

When the system is switched from STC to PSC1, CS system finds the optimal value around 0.12 after switching, and the optimal value is about 1934.9 W, however, oscillations occur at a later stage, leading to system instability; GWO-P&O system finds the optimal value around 0.66 s after switching, and the optimal value is about 1935.9 W; KOA-P&O system finds the optimal value around 0.6 s after switching, and the optimal value is about 1790.1 W, which is caught in the local optimum; IKOA-OIP&O system finds the optimal value around 0.38 s after switching, and the optimal value is about 1936.1 W. It can be seen that the accuracy of the system based on IKOA-OIP&O algorithm is better than the other three algorithms, and the speed of finding the optimal value still belongs to the top.

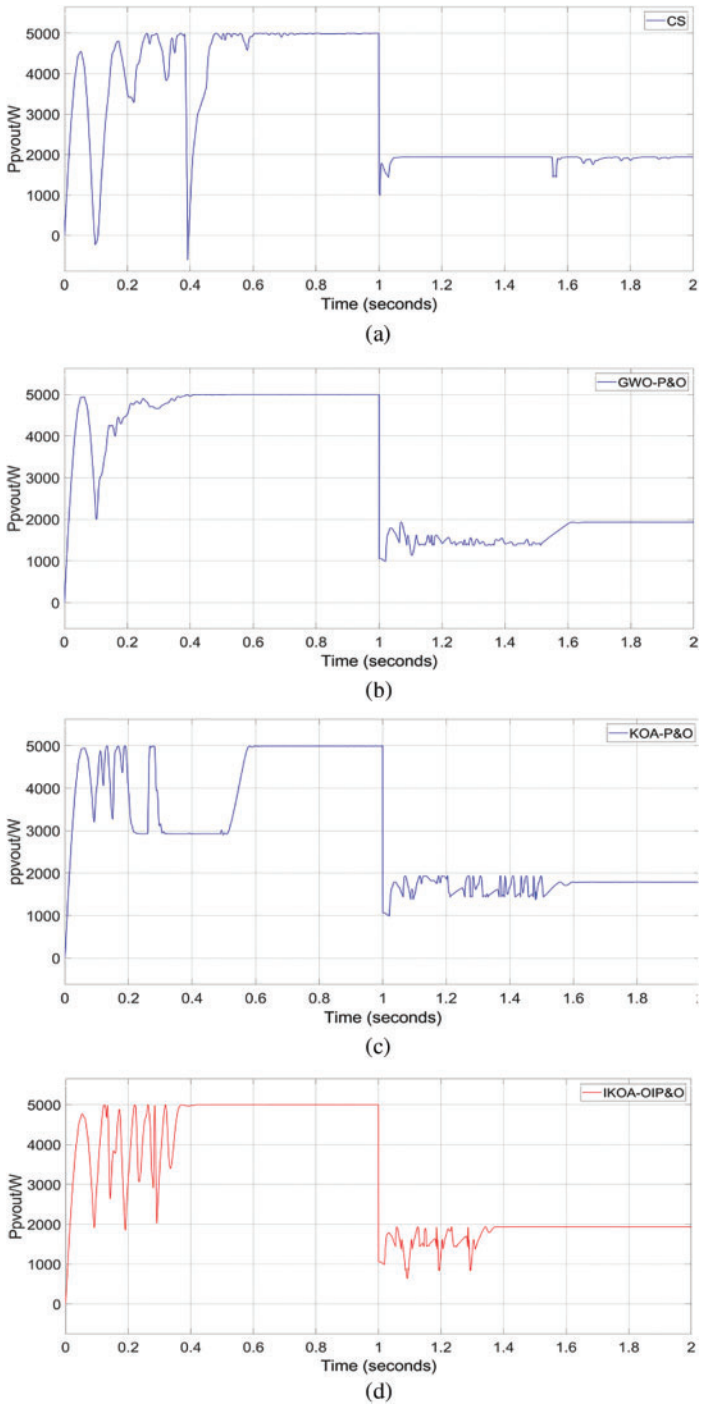

Figure 7: Comparison of algorithms under uniform light and partial shade conditions. (a) CS. (b) GWO-P&O. (c) KOA-P&O. (d) IKOA-OIP&O

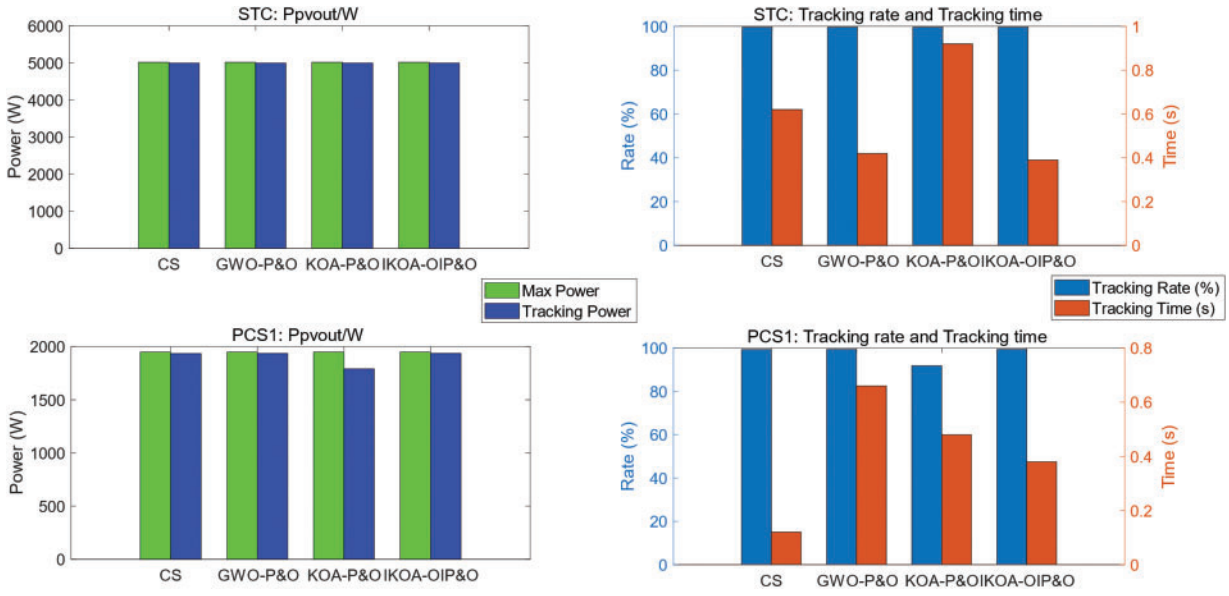

Figure 8: Comparison chart of algorithm results under STC-PSC1

5.2 Simulation Analysis under Dynamic Shade State Conditions

The natural shade environment is simulated by setting different light intensities, at which time the power output curve has multiple peaks, and it is easy to fall into possibility of local optimization when the peaks do not differ much. The power outputs of PSC1, PSC2 and PSC3 are shown in Fig. 5, and the maximum power in STC1 is 1948.3 W, the maximum power in STC2 is 1628.7 W, and the maximum power in STC3 is 3054.1 W. The simulation outputs are performed for the IKOA-OIPO algorithm, and the simulation outputs for the IKOA-OIPO algorithm, while the comparison with three algorithms, CS, GWO-P&O, and KOA-P&O, the results of the four algorithms are shown in Fig. 9, and the PSC1, PSC2, and PSC3 simulation results are shown in Table 5 and Fig. 10.

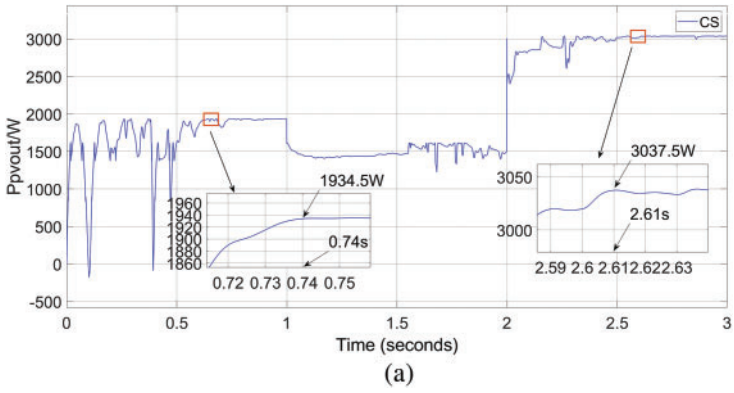

(a)

Figure 9: (Continued)

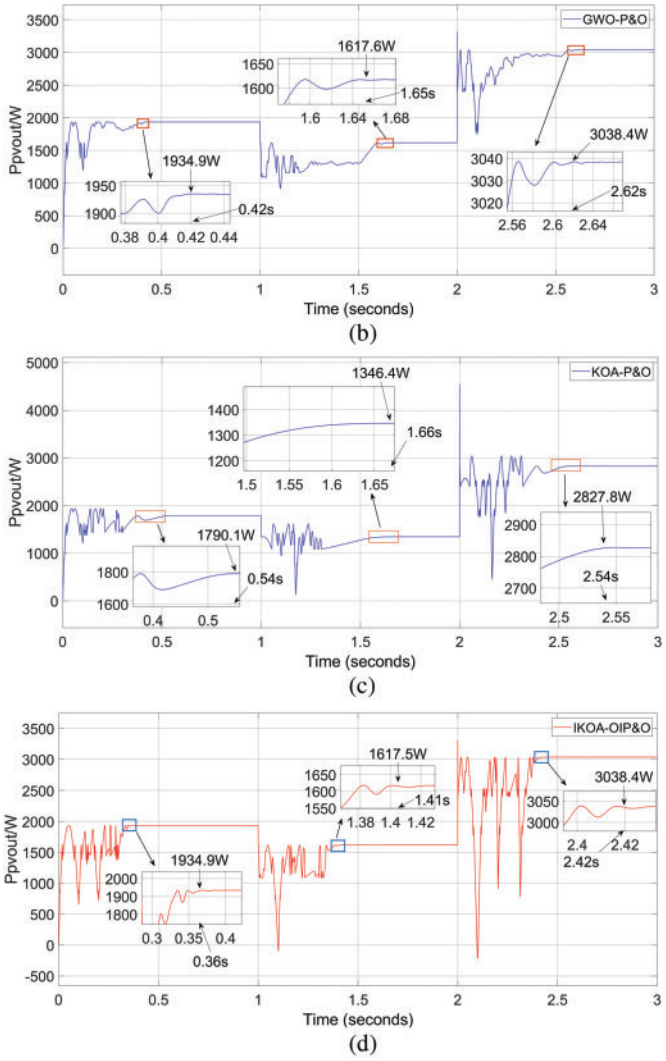

Figure 9: Comparison of algorithms in dynamic shade condition. (a) CS. (b) GWO-P&O. (c) KOA-P&O. (d) IKOA-OIP&O

From Figs. 9, 10 and Table 5, it can be seen that: in the initial PSC1 condition for MPPT, CS system finds the optimal value around 0.74 s of tracking, and the optimal value is around 1934.5 W; GWO-P&O system finds the optimal value around 0.42 s of tracking, and the optimal value is around 1934.9 W; KOA-P&O system finds the optimal value around 0.54 s and the optimal value is around 1934.9 W; IKOA-OIP&O system finds the optimal value around 0.36 s of tracing and the optimal value is around 1934.9 W.

When the simulation time reaches 1 s, PSC1 switches to PSC2, CS system initially falls into a local optimum during early tracking, but later becomes unstable due to multiple closely spaced peaks under condition two; GWO-P&O system finds the optimal value in the tracking of around 0.65 s, and the optimal value is around 1617.6 W; KOA-P&O system finds the optimal value around 0.66 s, and the optimal value is around 1346.4 W, but falls into the local optimum; IKOA-OIP&O system finds the optimal value around 0.41 s, and the optimal value is around 1617.5 W.

When simulation time reaches 2 s, PSC2 is switched to PSC3 condition, CS system finds the optimal value around the tracking 0.61 s process, and the optimal value is around 3037.5 W; the GWO-P&O system finds the optimal value around the tracking 0.62 s, and the optimal value is around 3038.4 W; KOA-P&O system finds the optimal value around the tracking 0.54 s, but falls into the local optimum; IKOA-OIP&O based on finds the optimal value around tracking around 0.42 s, and the optimal value is around 3038.4 W. In summary, the IKOA-OIP&O algorithm outperforms the other three algorithms in both speed and accuracy.

Table 5: Simulation results of the algorithm under dynamic shade condition

State mode	Algorithm	Maximum power/W	Tracking power/W	Tracking rate/%	Tracking time/s
PSC1	CS	1948.3	1934.5	99.29	0.74
	GWO-P&O	1948.3	1934.9	99.31	0.42
	KOA-P&O	1948.3	1934.9	99.31	0.54
	IKOA-OIP&O	1948.3	1934.9	99.31	0.36
PSC2	CS	1628.7	–	–	–
	GWO-P&O	1628.7	1617.6	99.32	0.65
	KOA-P&O	1628.7	1346.4	82.67	0.66
	IKOA-OIP&O	1628.7	1617.5	99.31	0.41
PSC3	CS	3054.1	3037.5	99.46	0.61
	GWO-P&O	3054.1	3038.4	99.49	0.62
	KOA-P&O	3054.1	2827.8	92.59	0.54
	IKOA-OIP&O	3054.1	3038.4	99.49	0.42

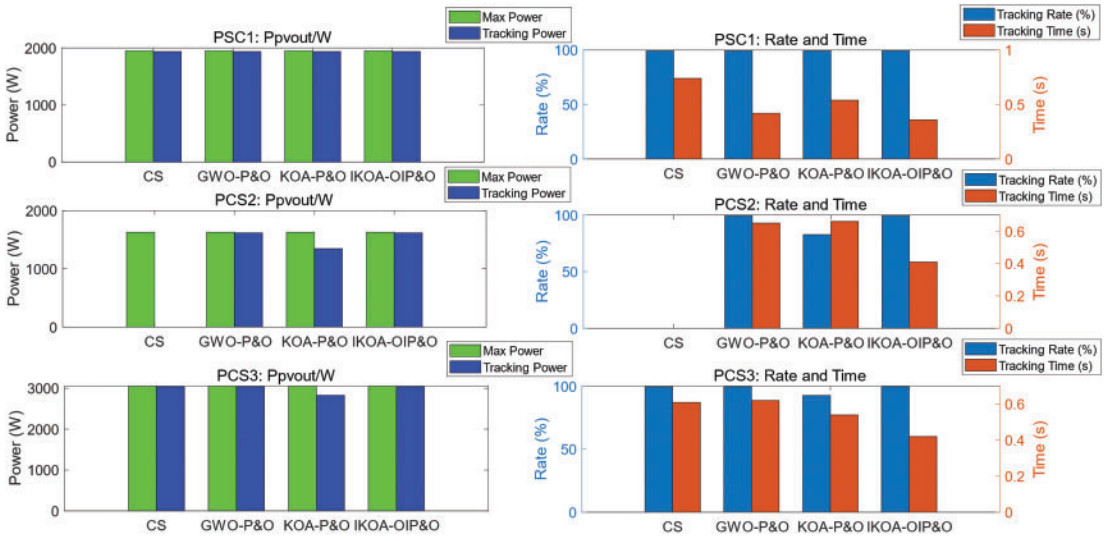

Figure 10: Comparison of algorithm results under PSC1-PSC2-PSC3

6 Conclusion

This paper proposes an MPPT optimization algorithm for PV systems in hybrid inverters, named the IKOA-OIP&O algorithm. This algorithm combines the IKOA with the OIP&O. The integration of algorithmic improvements and adaptive optimization coefficients enhances the MPPT accuracy and convergence speed.

Simulation analysis shows that compared to CS, GWO-P&O, and KOA-P&O algorithms with the same PV output sampling rate, IKOA-OIP&O exhibits stronger global search randomness in its early stages. Later, leveraging the OIP&O allows for swift local convergence, achieving up to 30% faster convergence time. Faster MPPT speeds enable the inverter to respond more quickly to changes in solar irradiance and temperature, thus optimizing power extraction in real time. This rapid adaptation minimizes energy losses and maximizes the energy harvested from the PV panels. More accurate MPPT tracking rates enhance the precision of power extraction by maintaining the inverter's operation at the true MPP. This precision ensures that the system operates efficiently even under fluctuating environmental conditions, leading to better overall system performance and energy yield. Improved MPPT accuracy also contributes to the stability and reliability of the energy storage system by preventing unnecessary power fluctuations and maintaining consistent energy flow to the grid or storage units. The algorithm mitigates power oscillations in PV outputs, showing stability and faster convergence in multi-state MPPs and single-state multi-peak shading conditions, making it suitable for MPPT in diverse shading scenarios.

The main contribution of this study is a systematic comparison of the performance of MPPT algorithms for single-and double-sided PV panels in hybrid PV inverters. Additionally, this study proposes an optimized MPPT strategy tailored for varying light conditions to enhance the dynamic responsiveness and accuracy of the MPPT algorithm, thereby improving overall power generation efficiency.

However, the algorithm has certain limitations. For instance, its performance may be compromised under extreme climatic conditions, such as high temperatures or significant shading. Additionally, challenges related to hardware deployment and computational resources may arise. Future research should address these limitations by enhancing the algorithm's robustness and computational efficiency to improve its applicability and performance across diverse environmental conditions.

Acknowledgement: The authors would like to thank and acknowledge the Jiangsu Key Laboratory of Power Transmission & Distribution Equipment Technology.

Funding Statement: The authors received funding from the Graduate Practice Innovation Program of Jiangsu University of Technology (XSJCX23_58), and Changzhou Science and Technology Support Project (CE20235045), and Open Project of Jiangsu Key Laboratory of Power Transmission & Distribution Equipment Technology (2021JSSPD12).

Author Contributions: The authors confirm contribution to the paper as follows: Study conception and design: Zhaoqiang Wang; data collection: Zhaoqiang Wang; analysis and interpretation of results: Zhaoqiang Wang; draft manuscript preparation: Zhaoqiang Wang and Fuyin Ni. All authors reviewed the results and approved the final version of the manuscript.

Availability of Data and Materials: The authors confirm that the data used in this study are available on request.

Ethics Approval: Not applicable.

Conflicts of Interest: The authors declare that they have no conflicts of interest to report regarding the present study.

References

[1] Z. Lin and S. Li, "A review of the current research situation of photovoltaic inverters," *Electric. Switchgear*, vol. 55, no. 5, pp. 10–13+18, 2017.

[2] J. A. Salim, M. S. Alwan, and B. M. Albaker, "A conceptual framework and a review of AI-based MPPT techniques for photovoltaic systems," *J. Phys.: Conf. Series*, vol. 1963, no. 1, 2021, Art. no. 12168. doi: 10.1088/1742-6596/1963/1/012168.

[3] K. Bao, H. Chen, Q. Cheng, and H. Wu, "Control method of photovoltaic energy storage Quasi-Z-source grid-connected inverter based on passive theory," *Smart Power*, vol. 50, no. 2, pp. 35–41, 2022.

[4] P. Ali and H. Constantine, "Employing load and irradiance profiles for the allocation of PV arrays with inverter reactive power and battery storage in distribution networks—A fast comprehensive QSTS technique," *Int. J. Electr. Power Energy Syst.*, vol. 130, 2021, Art. no. 106915. doi: 10.1016/J.IJEPES.2021.106915.

[5] A. Moses and H. Sun, "Bidirectional energy storage photovoltaic grid-connected inverter application system," *Int. J. Energy Res.*, vol. 44, no. 14, pp. 11509–11523, 2020. doi: 10.1002/er.5771.

[6] P. Padmavathi, N. Sudhakar, A. Belqasem, B. Karthik, and T. S. Babu, "PV-Fed micro-inverter with battery storage for single phase grid applications," *Elect. Power Compon. Syst.*, vol. 51, no. 11, pp. 1051–1074, 2023. doi: 10.1080/15325008.2023.2189758.

[7] L. de Oliveira-Assis *et al*., "Simplified model of battery energy-stored quasi-Z-source inverter-based photovoltaic power plant with Twofold energy management system," *Energy*, vol. 244, 2022, Art. no. 122563. doi: 10.1016/J.ENERGY.2021.122563.

[8] Y. Fan, J. Chen, Q. Bian, Y. Wu, J. Tong and C. Zhan, "Design of maximum power point energy storage and inverter for photovoltaic power generation," *J. Phys.: Conf. Series*, vol. 2771, no. 1, 2024, Art. no. 12018. doi: 10.1088/1742-6596/2771/1/012018.

[9] M. H. E. Banna, M. R. Hammad, A. I. Megahed, K. M. AboRas, A. Alkuhayli and N. Gowtham, "On-grid optimal MPPT for fine-tuned inverter based PV system using golf optimizer considering partial shading effect," *Alex. Eng. J.*, vol. 103, pp. 180–196, 2024. doi: 10.1016/j.aej.2024.05.115.

[10] B. Wang, W. Zhu, and Z. Bian, "Maximum power point tracking based on improved Cuckoo search algorithm combined with incremental conductance method," *Sci. Technol. Eng.*, vol. 24, no. 13, pp. 5388–5395, 2024.

[11] B. Yang, R. Xie, and Z. Guo, "Maximum power point tracking technology for PV systems: Current status and perspectives," *Energy Eng.*, vol. 121, no. 8, pp. 2009–2022, 2024. doi: 10.32604/ee.2024.049423.

[12] K. Guo, D. Yan, and J. Fu, "MPPT research of photovoltaic system based on improved perturbation and observation method," (in Chinese), *Chinese J. Power Sources*, vol. 45, no. 1, pp. 56–59, 2021.

[13] M. A. Bakar Siddique, A. Asad, R. M. Asif, A. U. Rehman, M. T. Sadiq and I. Ullah, "Implementation of incremental conductance MPPT algorithm with integral regulator by using boost converter in grid-connected PV array," *IETE J. Res.*, vol. 69, no. 6, pp. 3822–3835, 2023. doi: 10.1080/03772063.2021.1920481.

[14] C. B. Regaya, F. Farhani, H. Hamdi, A. Zaafouri, and A. Chaari, "A new MPPT controller based on a modified multiswarm PSO algorithm using an adaptive factor selection strategy for partially shaded PV systems," *Trans. Inst. Meas. Contr.*, vol. 46, no. 10, pp. 1991–2000, 2024. doi: 10.1177/01423312231225992.

[15] B. Liu, B. Chen, L. Qian, Y. Shi, and L. Lü, "Photovoltaic array power tracking strategy with an improved levy-flight grey wolf optimization and variable-step perturbation & observation," *J. Power Supply*, pp. 1–12, 2024.

[16] S. Sajid, H. M. Annas, J. M. Yaqoob, A. A. Bilal, and E. Krzysztof, "A horse herd optimization algorithm (HOA)-based MPPT technique under partial and complex partial shading conditions," *Energies*, vol. 15, no. 5, pp. 1880–1880, 2022. doi: 10.3390/en15051880.

[17] X. Liu, J. Zhu, H. Guo, and F. Bao, "Photovoltaic arrays MPPT method based on improved flower optimization algorithm," *Eng. J. Wuhan Univ.*, pp. 1–9, 2024.

[18] A. -B. Mohamed, M. Reda, A. S. A. Abdel, J. Mohammed, and A. Mohamed, "Kepler optimization algorithm: A new metaheuristic algorithm inspired by Kepler's laws of planetary motion," *Knowl. Based Syst.*, vol. 268, 2023, Art. no. 110454. doi: 10.1016/J.KNOSYS.2023.110454.

[19] H. -Q. Pablo, G. -T. Pablo, S. -M. Raúl, C. A. García-Vázquez, and L. M. Fernández-Ramírez, "Model predictive control of a microgrid with energy-stored quasi-Z-source cascaded H-bridge multilevel inverter and PV systems," *Appl. Energy*, vol. 346, 2023, Art. no. 121390. doi: 10.1016/J.APENERGY.2023.121390.

[20] A. Garrod and A. Ghosh, "A review of bifacial solar photovoltaic applications," *Front. Energy*, vol. 17, no. 6, pp. 704–726, 2023. doi: 10.1007/s11708-023-0903-7.

[21] M. H. Ibrahim, M. A. Ibrahim, and S. I. khather, "Modelling and analysis of SA-SPV system with bi-directional inverter for lighting load," *Przegląd Elektrotechniczny*, vol. 1, no. 5, pp. 128–131, 2022. doi: 10.15199/48.2022.05.23.

[22] C. Wang, "Research on three-phase bidirectional inverter based on Zeta-Sepic," M.S. thesis, Information Engineering, Nanchang Hangkong Univ, Nanchang, China, 2021.

[23] A. Musaed and R. Saifur, "A bi-level optimization method for voltage control in distribution networks using batteries and smart inverters with high wind and photovoltaic penetrations," *Int. J. Electr. Power Energy Syst.*, vol. 151, 2023, Art. no. 109217. doi: 10.1016/J.IJEPES.2023.109217.

[24] S. Han, J. Hu, Y. Han, J. Wang, L. Wang and P. Lund, "Research on modeling and power generation performance of bifacial photovoltaic module," *Acta Energiae Solaris Sinica*, vol. 44, no. 9, pp. 94–100, 2023. doi: 10.19912/j.0254-0096.tynxb.2022-0793.

[25] M. Tang *et al.*, "MPPT strategy of waterborne bifacial photovoltaic power generation system based on economic model predictive control," *Energies*, vol. 17, no. 1, 2023, Art. no. 152. doi: 10.3390/en17010152.

[26] F. Duan, M. Eslami, M. Khajehzadeh, A. Basem, D. J. Jasim and S. Palani, "Optimization of a photovoltaic/wind/battery energy-based microgrid in distribution network using machine learning and fuzzy multi-objective improved Kepler optimizer algorithms," *Sci. Rep.*, vol. 14, no. 1, 2024, Art. no. 13354. doi: 10.1038/s41598-024-64234-x.

[27] R. Mohamed, M. A. Basset, K. M. Sallam, I. M. Hezam, A. M. Alshamrani and I. A. Hameed, "Novel hybrid Kepler optimization algorithm for parameter estimation of photovoltaic modules," *Sci. Rep.*, vol. 14, no. 1, 2024, Art. no. 3453. doi: 10.1038/s41598-024-52416-6.

[28] X. Bai, S. Mo, S. Fan, L. Xu, and J. Xiong, "Research on MPPT control of photovoltaic systems based on NACS-PSO algorithm," *Electron. Meas. Technol.*, vol. 47, no. 3, pp. 62–70, 2024. doi: 10.19651/j.cnki.emt.2314795.